Spine

SPINE Volume 48, Number 5, pp E54–E69

BASIC SCIENCE

OPEN

miR-4478 Accelerates Nucleus Pulposus Cells Apoptosis Induced by Oxidative Stress by Targeting MTH1

Jiafang Zhang,[a,b] Ruiduan Liu,[c] Ling Mo,[d] Caijun Liu,[d] and Jianming Jiang, PhD[a]

Objectives. Low back pain is the leading cause of disability in the elderly population and is strongly associated with intervertebral disk degeneration (IVDD). However, the precise molecular mechanisms regulating IVDD remain elusive. This study aimed to investigate the role of differentially expressed miRNAs in the pathogenesis of IVDD.

Materials and Methods. We analyzed miRNA microarray datasets to identify differentially expressed miRNAs in IVDD progression and conducted quantitative real-time polymerase chain reaction and fluorescence in situ hybridization analysis to further confirm the differential expression of miR-4478 in nucleus pulposus (NP) tissues of patients diagnosed with IVDD. Using public databases of miRNA-mRNA interactions, we predicted the target genes of miR-4478, and subsequent flow cytometry and western blot analyses demonstrated the effect of MTH1 in H_2O_2-induced nucleus pulposus cells (NPCs) apoptosis. Finally, miR-4478 inhibitor was injected into NP tissues of the IVDD mouse model to explore the effect of miR-4478 in vivo.

Results. miR-4478 was upregulated in NP tissues from IVDD patients. Silencing of miR-4478 inhibits H_2O_2-induced NPCs apoptosis. MTH1 was identified as a target gene for miR-4478, and miR-4478 regulates H_2O_2-induced NPCs apoptosis by modulating MTH1. In addition, downregulation of miR-4478 alleviated IVDD in a mouse model.

Conclusions. In summary, our study provides evidence that miR-4478 may aggravate IVDD through its target gene MTH1 by accelerating oxidative stress in NPCs and demonstrates that miR-4478 has therapeutic potential in IVDD treatment.

Key words: intervertebral disk degeneration, microRNA, MTH1, oxidative stress, apoptosis

Spine 2023;48:E54–E69

Low back pain (LBP) is currently regarded as a leading cause of disability worldwide, resulting in a heavy global burden on the social economy and health services.[1] It has been reported that >80% of the population will experience LBP for more than four weeks in their lifetime, and 10% of them ultimately become disabled.[2–4] Intervertebral disk degeneration (IVDD) has been widely recognized as a main cause of LBP, but the existing understanding of the pathogenesis of IVDD is unsatisfactory.

The intervertebral disk (IVD), composed of an inner gel-like nucleus pulposus (NP) and an outer fibrocartilagenous annulus fibrosus (AF), is a flexible joint that connects adjacent vertebral bodies. Increased proinflammatory cytokines, a decreased number of nucleus pulposus cells (NPCs) in the extracellular matrix of the NP, and impaired cell activity are initial processes in an IVD degenerative cascade.[5,6] They result in the phenotypic transition of centrally located NPCs and consequently break the homeostasis between anabolism and catabolism. Previous studies indicated that reactive oxygen species (ROS) can change the microenvironment of NPCs, induce apoptosis and finally lead to IVDD.[7]

MicroRNAs (miRNAs or miRs) are a class of noncoding RNAs that play an important role in cell differentiation, proliferation, and apoptosis by mediating protein levels at the posttranscriptional level.[8] Abnormal expression of these proteins has been implicated in multiple degenerative diseases, including IVDD.[9,10] Zhang *et al*[11] reported that in human NP tissues, the expression level of miR-155 was negatively correlated with the degree of degeneration.

From the [a]Department of Orthopaedics, Division of Spine Surgery, Nanfang Hospital, Southern Medical University, Guangzhou, China; [b]Department of Orthopaedics, The Second Affiliated Hospital of Fujian University of Traditional Chinese Medicine, Fuzhou, China; [c]Affiliated Hospital of Guilin Medical University, Guilin, China; and [d]The Third Affiliated Hospital of Guangzhou University of Chinese Medicine, Guangzhou, China.

Acknowledgment date: January 20, 2022. First revision date: August 13, 2022. Acceptance date: August 31, 2022.

J.Z. and R.L. contributed equally to this work.

The authors report no conflicts of interest.

Address correspondence and reprint requests to Caijun Liu; Jianming Jiang, PhD; E-mails: liucaijun2005@163.com; jjm19991999@sohu.com

Supplemental Digital Content is available for this article. Direct URL citations appear in the printed text and are provided in the HTML and PDF versions of this article on the journal's website, www.spinejournal.com.

DOI: 10.1097/BRS.0000000000004486

Inhibition of miR-155 could upregulate MMP-16, which degrades proteoglycan and type II collagen fibers, thus leading to disk dehydration and degeneration. There have been a few successful phase I trials and numerous ongoing phase II/III trials that have manipulated miRNAs to treat diseases with complicated pathogenesis.

MutT homolog 1 (MTH1), also known as Nudix hydrolase 1 (NUDT1), or 7,8-dihydro-8-oxoguanine triphosphatase, is a member of the Nudix hydrolase family, and it is mainly distributed in the cytoplasm and mitochondria.[12,13] MTH1 can hydrolyze oxidized free nucleotides, such as 8-oxo-dGTP and 2-OH-dATP, to their monophosphate form and suppress their incorporation into the nucleus and mitochondrial DNA, thus preventing ROS-induced cell damage and death.[14–16] Previous studies have shown that MTH1 is capable of protecting several kinds of tumor cells from damage caused by high ROS levels. In hepatocellular carcinoma, a high level of ROS directly causes oxidative damage to DNA.[17] In return, liver cancer cells express high levels of MTH1 to limit ROS-related harmful effects, reduce apoptosis, and survive. In 2014, Gad *et al*[12] found that inhibition of MTH1 could reduce the proliferation ability of breast cancer, colon cancer, and osteosarcoma cancer cell lines and narrow the tumor to varying degrees. Whether MHT1 is involved in the process of IVDD by regulating the oxidative stress of disks and the underlying mechanisms of MTH1 in NPCs apoptosis is still unclear.

In this study, miR-4478 was identified as a degree-associated miRNA of IVDD using bioinformatics analysis. miR-4478 was shown to be most significantly upregulated. Subsequent experiments strongly suggested that miR-4478 might be involved in the mediation of the NPCs apoptotic pathway via MTH1-mediated oxidative stress. In summary, our study demonstrates miR-4478 as a potential therapeutic target for oxidative stress-induced IVDD.

MATERIALS AND METHODS

Ethics Statement

The current study was approved by the Medical Ethics Committee of the Nanfang Hospital of Southern Medical University and performed in strict accordance with the Declaration of Helsinki. Written informed consent was obtained from each donor or family member before tissue collection. Animal experiments were approved by the Medical Ethics Committee of the Nanfang Hospital of Southern Medical University.

NP Tissues Collection

Degenerative NP tissues were collected from 12 patients undergoing discectomy due to disk herniation. The control NP tissues were obtained from 12 patients with trauma (Table 1). Preoperative magnetic resonance imaging scans of the lumbar spine were routinely taken. According to the Pfirrmann classification, the degree of disk degeneration was graded from T2-weighted images by three independent observers. Patients with Pfirrmann grade I/II were assigned to the control group, while those with Pfirrmann grade III/IV/V constituted the degeneration group.

Gene Expression Omnibus Expression Datasets

The Gene Expression Omnibus (GEO) database (www.ncbi.nlm.nih.gov/geo/) is an international public repository that distributes high throughput gene expression datasets. To explore the differences of expression profiling and relevant biological processes in IVDD patients, we searched datasets from the GEO database with the keywords "intervertebral disk degeneration" [All Fields] AND "Homo sapiens"[porgn] AND "gse"[Filter] AND "2015/01"[Update Date]. The inclusion and exclusion criteria were as follows: datasets should be the whole-genome expression data of mRNA/miRNA; expression data should be obtained from human annulus disk tissue of IVDD patients and healthy controls. Finally, one mRNA expression datasets (GSE70362) and two miRNA expression datasets (GSE116726, GSE63492) were incorporated into our studies. The detail information of above-mentioned datasets was shown in Table 2. And the detail information of the top 10 dysregulated DEMis in GSE116726 and GSE63492 was shown in Table 3.

Microarray and Bioinformatics Analysis

The expression datasets were analyzed by the R software, version 4.0.0 (http://www.r-project.org). Briefly, after quantile normalization of the raw data, differentially expressed miRNAs with statistical significance between the two groups were identified through Volcano Plot filtering. Differentially expressed miRNAs between two samples were identified through fold change filtering. Hierarchical clustering was performed to show the distinguishable miRNA expression patterns among samples. The mRNA targets of miR-4478 were predicted using three programs: TargetScan (http://www.targetscan.org),[18] miRWalk (http://mirwalk.umm.uni-heidelberg.de/),[19] and miRDB (http://www.mirdb.org/index.html).[20] The detail information of above-mentioned results was shown in Table 4. Weighted correlation network analysis (WGCNA) was used to analyze the microarrays. A total of 122 genes from WGCNA were compiled with the targets of miR-4478. And then we used Kyoto Encyclopedia of Genes and Genomes (KEGG) and Gene Ontology (GO) enrichment analysis were performed by using the "ClusterProfiler" and "DOSE" R language packages to investigate the biological pathways that correlate with MTH1. We have uploaded the main code paths used in this article on github. For the detailed information, please refer to: https://github.com/articalcode/Spine.git.

Acquirement, Culture, and Treatment of NPCs

Human primary NPCs were purchased from Procell Life Science & Technology (Procell; Cat. #CP-H097). NPCs were cultured in Dulbecco's modified Eagle's medium (Gibco) and 10% fetal bovine serum (Biological Industries, Israel) supplemented with antibiotics (Gibco). The NPCs were

TABLE 1. Information of Human Disk Samples From 24 Patients

Human disk samples	Sex	Age (yr)	Diagnosis	Level	Grade
1	M	15	Trauma	T9/T10	I
2	F	16	Trauma	T7/T8	I
3	M	14	Trauma	T11/T12	I
4	F	13	Trauma	L2/L3	I
5	M	15	Trauma	L1/L2	I
6	F	17	Trauma	L3/L4	II
7	F	28	Trauma	L3/L4	II
8	F	36	Trauma	L4/L5	II
9	M	27	Trauma	L2/L3	II
10	M	39	Trauma	L3/L4	II
11	F	43	Trauma	L4/L5	II
12	F	34	Trauma	L4/L5	II
13	M	28	Disk herniation	L4/L5	III
14	M	31	Disk herniation	L2/L3	III
15	M	35	Disk herniation	L3/L4	III
16	M	42	Disk herniation	L3/L4	III
17	F	46	Disk herniation	L3/L4	IV
18	F	47	Disk herniation	L4/L5	IV
19	M	53	Disk herniation	L4/L5	IV
20	F	49	Disk herniation	L4/L5	IV
21	F	80	Disk herniation	L5/S1	V
22	F	79	Disk herniation	L2/L3	V
23	M	71	Disk herniation	L3/L4	V
24	M	67	Disk herniation	L2/L3	V

F indicates female; M, male.

passaged twice or three times before experiments. To induce oxidative stress-induced apoptosis, cells were treated with 100 μM H_2O_2 for 12 hours before experiments. NPCs viability was measured using a CCK8 assay (Dojindo Molecular Technologies Inc.) following the manufacturer's instructions. The absorbance of the wells was measured at 450 nm.

RNA Isolation and Quantitative Real-time Polymerase Chain Reaction

Total RNA, including miRNA, from NP tissues or cultured cells was isolated with TRIzol Reagent (Invitrogen) according to the manufacturer's instructions. RNA quantity was analyzed using a Nanodrop (Thermo Scientific). The mRNA was reverse transcribed into complementary DNA using a reverse transcription kit (Takara; Cat. #RR047A). The miRNA was reverse transcribed using a miRNA first-strand complementary DNA synthesis kit (Sangon; Cat. #B532451-0020). Relative expression levels were calculated by the $2^{-\Delta\Delta C_t}$ method. U6 and glyceraldehyde 3-phosphate dehydrogenase (GAPDH) were used to normalize miRNA and mRNA expression levels, respectively. The following primers were used: human MTH1 (F: 5′-GAGCGGCGGTGCA-

TABLE 2. Information of Microarray Datasets

Dataset	Control	IVDD	Platform	Year	Country	Author	PMID
mRNA expression profiling (14 control *vs.* 10 IVDD)							
GSE70362	14	10	GPL17810 (HG-U133_Plus_2) Affymetrix Human Genome U133 Plus 2.0 Array	2015	Ireland	Peadar O'Gaora	26489762
miRNA expression profiling (8 control *vs.* 8 IVDD)							
GSE116726	3	3	GPL20712 Agilent-070156 Human miRNA (miRNA version)	2018	China	Jian Chen	30487517
GSE63492	5	5	GPL19449 Exiqon miRCURY LNA microRNA array, 7th generation REV—hsa, mmu, and rno (miRBase v18.0)	2016	China	Haiqiang Wang	26484230

IVDD indicates intervertebral disk degeneration.

TABLE 3. Top 10 Dysregulated Differentially Expressed MicroRNAs in GSE116726 and GSE63492

	GSE63492		GSE116726	
miRNA	**Fold change**	***P***	**Fold change**	***P***
hsa-miR-10b-5p	1.473198	0.02624	1.735719	3.77E−07
hsa-miR-185-5p	1.710294	0.00716	1.540509	1.93E−05
hsa-miR-4306	1.925335	0.000588	1.737333	0.000177
hsa-miR-4434	1.530412	0.007267	−1.70726	1.43E−08
hsa-miR-4478	1.24586	0.011455	1.715781	4.76E−05
hsa-miR-4533	1.237034	0.00591	−1.17896	5.87E−07
hsa-miR-4674	1.838539	0.004679	−1.69685	2.85E−07
hsa-miR-486-5p	1.831134	0.006747	2.846687	1.27E−07
hsa-miR-5100	1.972121	0.008841	1.604745	5.82E−06
hsa-miR-663a	−1.32409	0.011362	1.464256	0.000164

GAACCCAG-3′, R: 5′-AGAAGACATGCACGTCCATG AG-3′); human GAPDH (F: 5′-GACAGTCA-GCCGCA TCTTCTT-3, R: 5′-AATCCGTTGACTCCGACCTTC-3′). GAPDH was used for normalization.

Fluorescence In Situ Hybridization

A locked nucleic acid probe with complementarity to miR-4478 was labeled with 5′ and 3′-digoxigenin and synthesized by Exiqon (Woburn). A scrambled locked nucleic acid probe was used as a negative control. The NP tissues from IVDD patients were used for fluorescence in situ hybridization (FISH) detection. The slides were prehybridized for 30 minutes at 52 °C and then 10 pmol of the probe in hybridization mixture was added to each slide and incubated for one hour at 52 °C. After washing, slides were incubated in blocking buffer for 30 minutes at room temperature, then antibody was added, and slides were incubated for 30 minutes at room temperature. The TSA Plus Fluorescein System (PerkinElmer) was used for direct fluorescence detection according to the manufacturer's protocol. The slides were imaged using an epifluorescence microscope equipped with charge-coupled device camera and image analysis capabilities. Tissue sections were mounted in Vectashield (Vector Laboratories). Images were taken with FV1000 confocal laser scanning microscope (Olympus IX-81; Olympus).

Immunohistochemical Staining

The disks from humans and mice were fixed in 4% paraformaldehyde for one week, decalcified in 20% EDTA for two weeks, paraffin-embedded, and then carefully sectioned to a 7 μm thickness. After deparaffinization, antigen retrieval, and blocking with 5% goat serum, the slides were incubated with primary antibody: MTH1 (diluted 1:200, Cat. #ab197028; Abcam) and secondary antibody (DAKO). Subsequently, sections were developed with DAB solution (DAKO, Denmark) and then counterstained with hematoxylin. Histological images were acquired using an Olympus BX63 microscope (Olympus) with randomly selected fields in each section at ×400 magnification. The percentages of $MTH1^+$ cells were quantified using ImageJ software (National Institutes of Health). We considered <50% positive staining as low expression of MTH1 and ≥50% positive staining as high expression of MTH1.

Cell Transfection

NPCs were seeded in six-well plates for 24 hours (5×10^5/well) and then transfected with oligonucleotides or vectors (mimics NC: 5′-GUCAGCCUGCUGAGGAG-3′, miR-4478 mimics: 5′-GAGGCUGAGCUGAGGAG-3′, inhibitor NC: 5′-CUCCUCAGCAGGCUGAC-3′, and miR-4478 inhibitor: 5′-CUCCUCAGCUCAGCCUC-3′) (RiboBio Co. Ltd) at 50 nM using Lipofectamine RNAiMAX Transfection Reagent (Invitrogen). To suppress MTH1 expression, NPCs were transfected with either MTH1 siRNA or control scrambled siRNA (RiboBio Co. Ltd) using Lipofectamine 3000 (Invitrogen) according to the manufacturer's instructions. After 48 hours of treatment, the cellular lysates were collected to analyze the expression of genes of interest. The following siRNA sequences were used: MTH1 siRNA #1 5′-GACGACAGCUACUGGUUUC-3′; MTH1 siRNA #2 5′-CGACGACAGCUACUGGUUU-3′.

Dual-luciferase Reporter Assay

A synthesized MTH1 3′ untranslated region gene fragment, including the predicted miR-4478-binding site, was inserted into a luciferase vector (Promega). The vectors, miR-4478, and luciferase vector were confirmed using RNA sequencing and then cotransfected into NPCs, which were seeded in a 96-well plate at 5×10^3 cells per well. The cellular lysates were collected 48 hours after transfection, and luciferase activity was measured with the Dual-Luciferase Reporter Assay System (Promega) according to the manufacturer's instructions.

Flow Cytometry

The NPCs were harvested by 0.25% trypsin (Gibco Life Technologies) and then stained using an Annexin V-FITC Apoptosis Detection Kit (BD) according to the manufacturer's instructions. Briefly, NPCs were washed twice

TABLE 4. Predicted Target Genes of miR-4478 by TargetScan, miRDB and miRWalk

Gene	Representative miRNA	CWC score	TC score	Start	End	TargetScan	miRDB
AAK1	hsa-miR-4478	−0.11	−0.13	11,461	11,483	1	1
ABHD17A	hsa-miR-4478	−0.27	−0.27	27	50	1	0
ABHD17B	hsa-miR-4478	−0.49	−0.49	275	316	1	1
AFF3	hsa-miR-4478	−0.27	−0.28	1258	1276	1	1
ARHGAP44	hsa-miR-4478	−0.16	−0.21	2848	2865	1	1
ARHGAP5	hsa-miR-4478	−0.25	−0.31	1622	1640	1	1
ARID4B	hsa-miR-4478	−0.38	−0.39	4448	4465	1	1
ARMC8	hsa-miR-4478	−0.32	−0.32	3830	3858	1	1
ASB4	hsa-miR-4478	−0.26	−0.26	2037	2071	1	0
ATXN7L3	hsa-miR-4478	−0.25	−0.27	2094	2149	1	0
B3GAT2	hsa-miR-4478	−0.05	−0.05	784	819	1	0
B3GNT9	hsa-miR-4478	-0.11	-0.11	779	820	1	0
BCORL1	hsa-miR-4478	−0.09	−0.21	3560	3613	1	1
BTAF1	hsa-miR-4478	−0.54	−0.55	2991	3009	1	1
BZW1	hsa-miR-4478	−0.03	−0.05	4357	4382	1	0
C1orf21	hsa-miR-4478	−0.03	−0.31	7918	7952	1	0
CADM1	hsa-miR-4478	0	−0.45	8322	8352	1	1
CAPRIN1	hsa-miR-4478	−0.16	−0.18	536	557	1	0
CCDC85C	hsa-miR-4478	−0.05	−0.41	12,175	12,196	1	1
CD47	hsa-miR-4478	−0.1	−0.24	1840	1860	1	0
CDH11	hsa-miR-4478	−0.06	−0.06	4522	4555	1	0
CDH7	hsa-miR-4478	−0.34	−0.48	1821	1856	1	1
CDK4	hsa-miR-4478	−0.18	−0.43	911	930	1	1
CELSR3	hsa-miR-4478	−0.01	−0.01	9850	9872	1	1
CNKSR2	hsa-miR-4478	−0.22	−0.24	1615	1642	1	1
COL6A6	hsa-miR-4478	−0.36	−0.36	1436	1486	1	1
COPS7B	hsa-miR-4478	−0.36	−0.36	1298	1322	1	1
CSPG5	hsa-miR-4478	−0.61	−0.61	1816	1835	1	1
CTDSPL2	hsa-miR-4478	−0.35	−0.35	1538	1557	1	1
CXCR5	hsa-miR-4478	−0.19	−0.19	1200	1242	1	0
CYTIP	hsa-miR-4478	0	−0.28	895	911	1	0
DAAM1	hsa-miR-4478	−0.16	−0.23	1319	1346	1	1
DCBLD2	hsa-miR-4478	−0.22	−0.22	2083	2104	1	0
DNAJB1	hsa-miR-4478	−0.03	−0.06	280	301	1	0
DNAJC21	hsa-miR-4478	−0.15	−0.42	5324	5370	1	1
DOCK3	hsa-miR-4478	−0.25	−0.25	4400	4425	1	1
EPB41L1	hsa-miR-4478	−0.12	−0.15	5194	5256	1	1
FAM83G	hsa-miR-4478	−0.07	−0.07	4363	4410	1	0
FASTK	hsa-miR-4478	−0.2	−0.2	260	283	1	0
FBN1	hsa-miR-4478	−0.13	−0.13	3266	3292	1	1
FGF9	hsa-miR-4478	−0.27	−0.29	998	1049	1	1
FLRT2	hsa-miR-4478	−0.23	−0.3	17,662	17,691	1	0
FNIP2	hsa-miR-4478	−0.11	−0.18	2640	2669	1	0
FOXO1	hsa-miR-4478	−0.52	−0.52	1874	1896	1	1
GAB2	hsa-miR-4478	−0.05	−0.05	3207	3246	1	1
GABRB3	hsa-miR-4478	−0.04	−0.46	1229	1250	1	1
GAPVD1	hsa-miR-4478	−0.03	−0.2	7233	7270	1	0
GOLGA3	hsa-miR-4478	−0.2	−0.22	2616	2637	1	1
GPR153	hsa-miR-4478	−0.37	−0.37	2674	2697	1	1
GRIN2A	hsa-miR-4478	0	−0.02	3578	3604	1	0

TABLE 4. (*Continued*)

GRIN3A	hsa-miR-4478	−0.02	−0.02	110	148	1	0
GUCY1A2	hsa-miR-4478	−0.04	−0.21	1916	1962	1	0
GXYLT1	hsa-miR-4478	−0.12	−0.16	3000	3022	1	1
HAT1	hsa-miR-4478	−0.51	−0.51	3294	3329	1	1
HECW2	hsa-miR-4478	−0.05	−0.05	88	113	1	0
IGF1	hsa-miR-4478	−0.14	−0.43	421	452	1	1
IL23R	hsa-miR-4478	−0.21	−0.21	2716	2753	1	0
INPP5K	hsa-miR-4478	−0.13	−0.31	2745	2793	1	0
IPO7	hsa-miR-4478	−0.05	−0.05	2595	2614	1	0
IRX5	hsa-miR-4478	−0.14	−0.34	1065	1087	1	0
KCNJ15	hsa-miR-4478	−0.05	−0.05	1492	1516	1	0
KCNQ3	hsa-miR-4478	−0.12	−0.12	9672	9691	1	1
KDM5B	hsa-miR-4478	−0.09	−0.09	3008	3040	1	1
KLHDC10	hsa-miR-4478	−0.11	−0.13	184	209	1	0
MAML2	hsa-miR-4478	−0.07	−0.09	1484	1507	1	0
MAML3	hsa-miR-4478	−0.27	−0.27	3960	3985	1	1
MARK1	hsa-miR-4478	−0.24	−0.25	538	576	1	1
MTH1	hsa-miR-4478	−0.31	−0.31	262	268	1	1
NCKAP5	hsa-miR-4478	−0.14	−0.32	4426	4448	1	1
NFAT5	hsa-miR-4478	−0.05	−0.07	2840	2876	1	0
NFYA	hsa-miR-4478	−0.12	−0.21	266	286	1	0
NR2C2	hsa-miR-4478	−0.18	−0.28	7354	7381	1	1
PDE4A	hsa-miR-4478	−0.08	−0.08	631	659	1	1
PIK3R1	hsa-miR-4478	−0.3	−0.32	4977	4994	1	1
PIM1	hsa-miR-4478	−0.44	−0.44	69	94	1	0
PLAGL2	hsa-miR-4478	−0.12	−0.45	4488	4514	1	1
PLXNA4	hsa-miR-4478	−0.05	−0.06	200	234	1	1
POU2F1	hsa-miR-4478	−0.02	−0.02	383	436	1	0
PRRC2C	hsa-miR-4478	−0.24	−0.24	7882	7906	1	1
PSMB5	hsa-miR-4478	−0.01	−0.05	594	631	1	0
PTEN	hsa-miR-4478	−0.28	−0.34	237	286	1	1
RAP1A	hsa-miR-4478	−0.17	−0.17	2590	2615	1	0
RAPGEFL1	hsa-miR-4478	−0.21	−0.21	2436	2470	1	0
RASSF3	hsa-miR-4478	−0.33	−0.36	828	891	1	1
RBM12	hsa-miR-4478	−0.16	−0.38	2284	2305	1	0
RNF125	hsa-miR-4478	−0.01	−0.01	2261	2286	1	0
SCNM1	hsa-miR-4478	0	−0.18	70	105	1	1
SEMA3A	hsa-miR-4478	−0.26	−0.27	4880	4897	1	1
SHB	hsa-miR-4478	−0.08	−0.21	2427	2448	1	0
SLC12A5	hsa-miR-4478	−0.15	−0.15	3957	4009	1	1
SLC4A8	hsa-miR-4478	−0.06	−0.09	5569	5593	1	0
SMAD2	hsa-miR-4478	−0.23	−0.29	4873	4896	1	1
SMARCD2	hsa-miR-4478	−0.26	−0.26	487	510	1	0
SORCS1	hsa-miR-4478	−0.26	−0.28	4071	4087	1	0
SOX12	hsa-miR-4478	−0.12	−0.12	4448	4468	1	0
SP5	hsa-miR-4478	−0.42	−0.45	1077	1102	1	1
SPATS2L	hsa-miR-4478	0	−0.15	2034	2073	1	0
SRPK2	hsa-miR-4478	0	−0.28	1173	1194	1	0
SRSF3	hsa-miR-4478	−0.59	−0.59	3979	4028	1	1
ST6GALNAC6	hsa-miR-4478	−0.32	−0.52	2336	2386	1	1
STK4	hsa-miR-4478	−0.2	−0.21	1917	1952	1	1
SURF2	hsa-miR-4478	0	−0.12	703	729	1	0

TABLE 4. (*Continued*)

TANC1	hsa-miR-4478	−0.21	−0.22	2616	2635	1	1
TBL1X	hsa-miR-4478	−0.09	−0.09	3	27	1	0
TENM1	hsa-miR-4478	−0.12	−0.12	5369	5392	1	0
TENM2	hsa-miR-4478	−0.25	−0.25	7415	7435	1	1
TET3	hsa-miR-4478	−0.04	−0.04	6132	6156	1	1
TMEM115	hsa-miR-4478	−0.11	−0.11	1891	1915	1	1
TMEM178B	hsa-miR-4478	−0.02	−0.02	5983	6007	1	1
TMOD1	hsa-miR-4478	−0.09	−0.18	2407	2448	1	0
TRHDE	hsa-miR-4478	−0.17	−0.3	461	482	1	0
TRPM3	hsa-miR-4478	−0.01	−0.01	1837	1879	1	0
TWF1	hsa-miR-4478	−0.48	−0.48	1167	1185	1	1
TXLNG	hsa-miR-4478	−0.3	−0.3	91	141	1	1
UBE2N	hsa-miR-4478	−0.04	−0.44	2021	2063	1	1
UNC5C	hsa-miR-4478	−0.14	−0.14	8629	8656	1	1
ZNF207	hsa-miR-4478	−0.01	−0.02	12,513	12,538	1	0
ZNF507	hsa-miR-4478	−0.01	−0.05	1904	1922	1	0
ZNF740	hsa-miR-4478	−0.32	−0.33	1203	1240	1	1
ZNF827	hsa-miR-4478	−0.12	−0.29	1872	1893	1	1
ZNRF2	hsa-miR-4478	−0.03	−0.46	746	767	1	0
ZZZ3	hsa-miR-4478	−0.02	−0.02	2967	2996	1	0

CWC indicates cumulative weighted context; TC, total context.

with cold phosphate-buffered saline and resuspended in 100 μL of binding buffer at a concentration of 1×10^6 cells/mL. After incubation with 5 μL of Annexin V-fluorescein isothiocyanate (FITC) solution and 5 μL of propidium solution (PI) for 15 minutes at room temperature, the NPCs were analyzed by flow cytometry (Beckman Coulter). The early apoptotic cells were Annexin V-FITC+/PI–, late apoptotic cells were Annexin V-FITC+/PI+, and normal cells were Annexin V-FITC–/PI–.

Western Blotting

Total protein was extracted from human NP specimens or from cultured primary human NPCs using RIPA buffer supplemented with protease and phosphatase inhibitors and phenylmethylsulfonyl fluoride (PMSF). The protein concentrations were measured by a BCA Protein Assay Reagent Kit (KeyGEN BioTECH). The lysates were loaded (20 μg per well), separated on 10% sodium dodecyl sulfate-polyacrylamide gels (Epizyme Biotech), and then transferred to 0.22 μm PVDF membranes (Millipore) by electroblotting. The membranes were blocked with 3% bovine serum albumin in TBS-T for two hours and then incubated with the following primary antibodies at 4 °C overnight: anti-MTH1 (diluted 1:1000, Cat. #ab200832; Abcam), anti-Bax (diluted 1:1000, Cat. #ab182733; Abcam), anti-Bcl-2 (diluted 1:1000, Cat. #ab182858; Abcam), anti-cleaved-caspase 3 (diluted 1:1000, Cat. #ab32042; Abcam), and anti-beta actin antibodies (diluted 1:1000, Cat. # ab8226; Abcam). After being washed with TBS-T, the membranes were incubated with HRP-linked anti-rabbit immunoglobulin G (IgG; diluted 1:1000, Cat. #7074; Cell Signaling Technology) for two hours. Subsequently, protein bands were detected with enhanced chemiluminescence reagents (Millipore). The results of this experiment were quantified using a multigauge densitometry system (Fujifilm).

Mouse Model of IVDD

The IVDD model was established in C57BL/6 mice by AF needle puncture as described in previous study.[21–24] In short, general anesthesia was administered using pentobarbital sodium (100 mg/kg). A midline abdominal incision was made in the front to visualize the L3/L4 IVDs. A 27 G needle was inserted into the L3–L4 disk parallel to the endplates by 1.5 mm, rotated in the axial direction by 180°, and held for 30 seconds, and a vessel clamp was used to grip on the marker on the needle to control the depth. No treatment was performed on the mice in the control group. Then the miRNA inhibitor solution was administrated following the manufacturer's instructions. Briefly, 2 μL of phosphate-buffered saline with 10 nM of miR-4478 inhibitor or inhibitor control was delivered into the punctured disk through an intradiscal injection via a 33 G Hamilton syringe (Hamilton Co.). Subsequently, we used 3-0 silk sutures to close the muscles, and 4-0 nylon sutures to close the skin margins. Lumbar magnetic resonance imaging examinations were performed on the mice eight weeks after the operation. All disks were harvested after magnetic resonance imaging examinations for further experiments.

The Criteria of Histological Scores

A mouse disk histological scoring system was used to help assess the degree of IVDD.[25] It took NP structure, NP clefts/

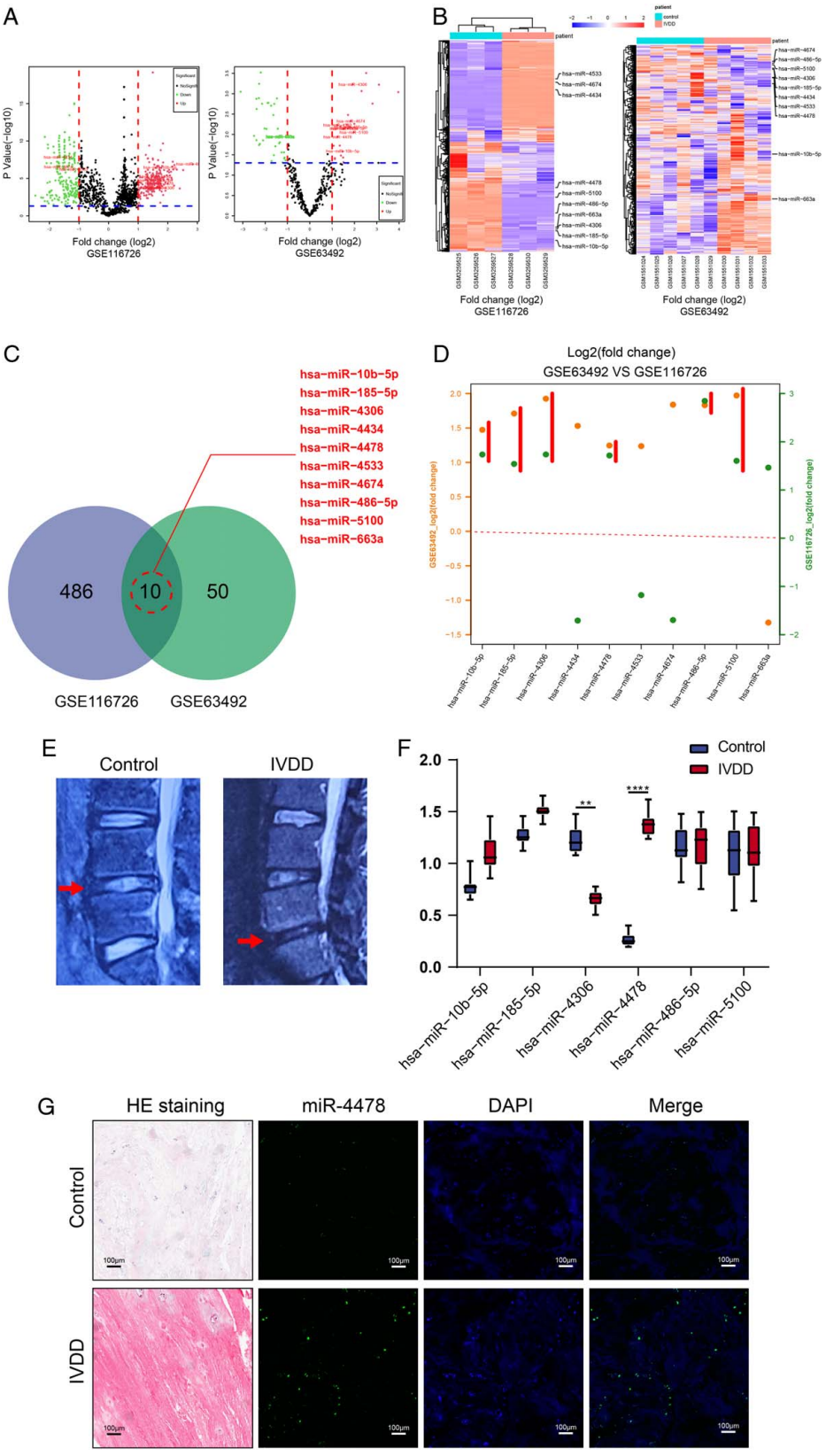
A
P Value(−log10)
Fold change (log2)
GSE116726
Fold change (log2)
GSE63492
B
patient
control
IVDD
hsa−miR−4533
hsa−miR−4674
hsa−miR−4434
hsa−miR−4478
hsa−miR−5100
hsa−miR−486−5p
hsa−miR−663a
hsa−miR−4306
hsa−miR−185−5p
hsa−miR−10b−5p
Fold change (log2)
GSE116726
Fold change (log2)
GSE63492
C
hsa−miR−10b−5p
hsa−miR−185−5p
hsa−miR−4306
hsa−miR−4434
hsa−miR−4478
hsa−miR−4533
hsa−miR−4674
hsa−miR−486−5p
hsa−miR−5100
hsa−miR−663a
486
10
50
GSE116726
GSE63492
D
Log2(fold change)
GSE63492 VS GSE116726
GSE63492_log2(fold change)
GSE116726_log2(fold change)
E
Control
IVDD
F
Control
IVDD
**
****
hsa−miR−10b−5p
hsa−miR−185−5p
hsa−miR−4306
hsa−miR−4478
hsa−miR−486−5p
hsa−miR−5100
G
HE staining
miR-4478
DAPI
Merge
Control
IVDD
100μm

Figure 1. miR-4478 was upregulated in NP tissues from IVDD patients. (A) Volcano plots showed differentially expressed miRNAs between IVDD patients and controls in GSE116726 and GSE63492. Note: GSE116726 (IVDD = 3; control = 3) and GSE63492 (IVDD = 5; control = 5). (B) Heatmap illustrated the top 10 differentially expressed miRNAs in GSE116726 and GSE63492. (C) Venn diagram depicted the top 10 differentially expressed miRNAs in IVDD that were identified based on the overlap of GSE116726 and GSE63492. (D) Scatter plot showed that six out of 10 miRNAs were upregulated both in GSE116726 and GSE63492. (E) The representative magnetic resonance images of IVDD patients and controls. In this group of pictures, as indicated by red arrows, the control sample graded as Pfirrmann grade II was obtained from L4/L5, and the IVDD sample graded as Pfirrmann grade V was obtained from L5/S1. (F) Compared with controls (n = 12), the miR-4478 expression level was significantly upregulated in IVDD patients (n = 12). $^{**}P < 0.01$, $^{****}P < 0.0001$. (G) The representative HE staining images of IVDD patients and controls; fluorescence in situ hybridization analysis of NP tissues from IVDD patients demonstrated an increased level of miR-4478 (scale bar = 50 μm). Data shown as mean ± SD. HE indicates hematoxylin and eosin; IVDD, intervertebral disk degeneration; NP, nucleus pulposus.

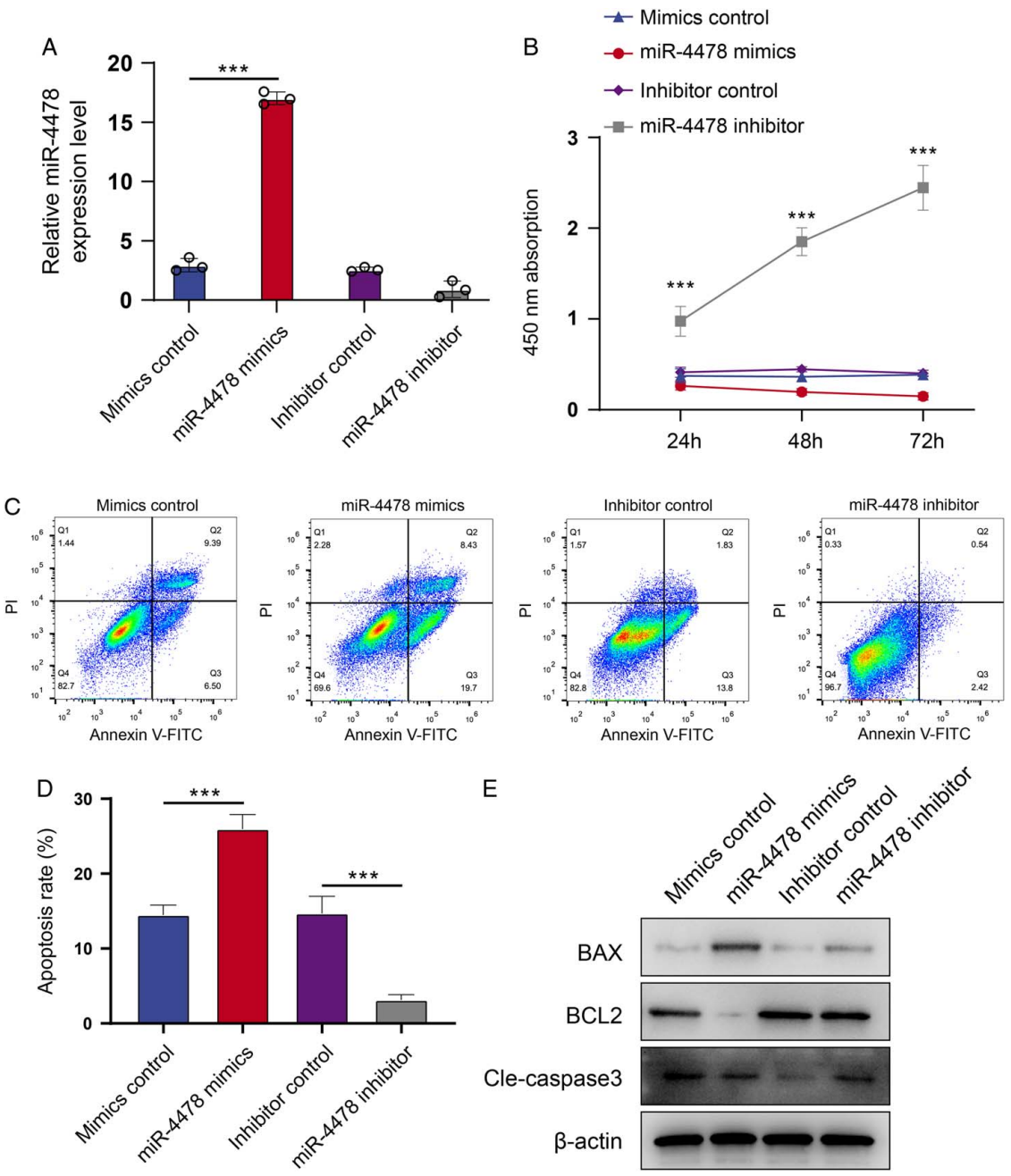

Figure 2. Silencing of miR-4478 inhibits H_2O_2-induced nucleus pulposus cells (NPCs) apoptosis. (A) Forty-eight hours after transfected with miR-4478 mimics or inhibitor or their negative control, the NPCs were used for the following experiments. Transfection efficiency of miR-4478 was analyzed by quantitative real-time polymerase chain reaction (n = 3 replicates per group). $^{***}P < 0.001$. (B) Cell proliferation was analyzed in above-mentioned NPCs by CCK8 (n = 3 replicates per group). $^{***}P < 0.001$. (C and D) Analysis of NPCs apoptosis was assayed by flow cytometry (n = 3 replicates per group). miR-4478 promoted H_2O_2-induced apoptosis in NPCs. $^{***}P < 0.001$. (E) The expression levels of BAX, BCL2, and cleaved caspase 3 in NPCs were detected by western blot. All groups in C–E were treat with 100 μM H_2O_2 for 12 hours after transfected with miR-4478 mimics or inhibitor or their negative control for 48 hours.

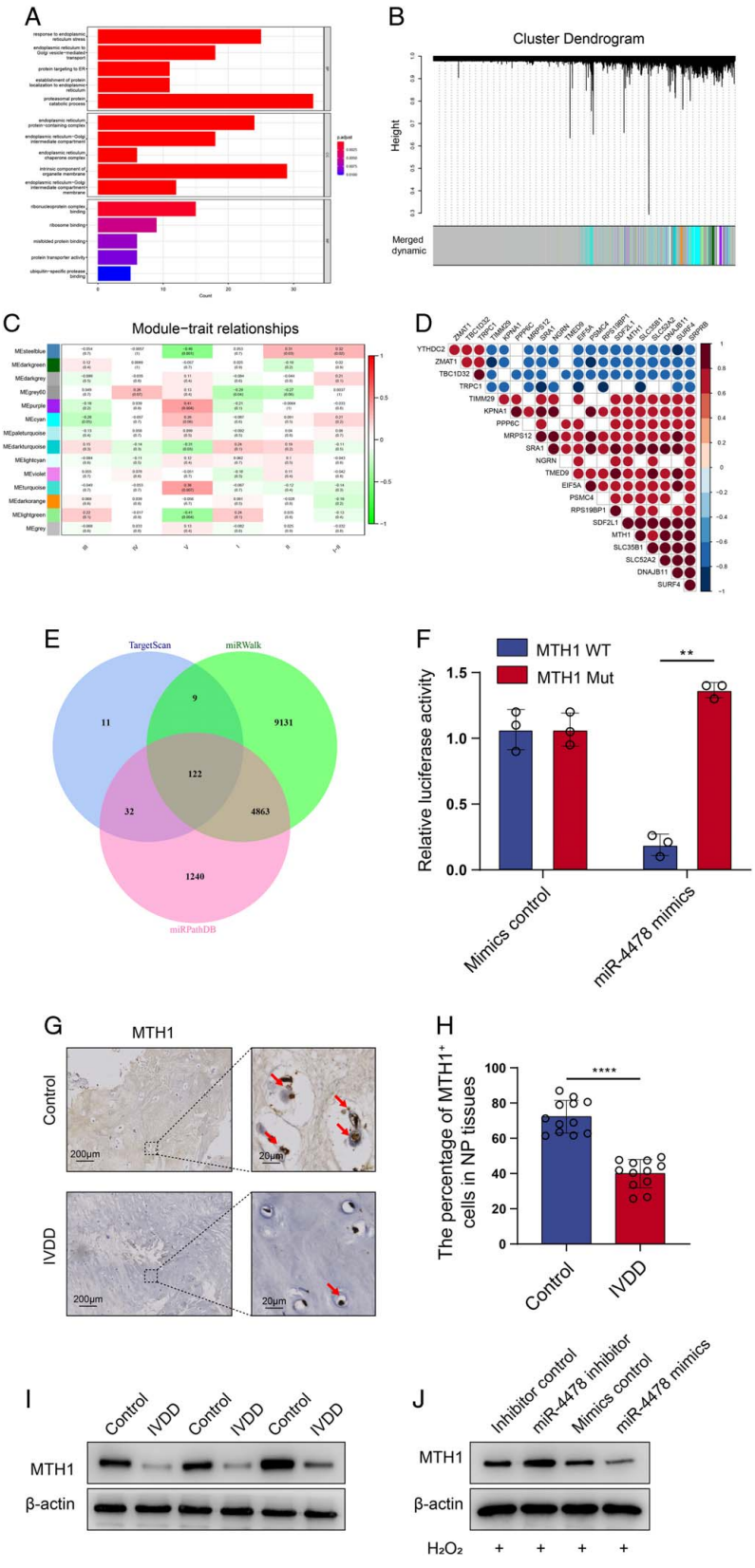
A
B
Cluster Dendrogram
Height
Merged dynamic
C
Module−trait relationships
D
E
TargetScan
miRWalk
miRPathDB
11
9
9131
122
32
4863
1240
F
MTH1 WT
MTH1 Mut
**
Relative luciferase activity
Mimics control
miR-4478 mimics
G
MTH1
Control
IVDD
200μm
20μm
H
****
The percentage of MTH1+ cells in NP tissues
Control
IVDD
I
Control
IVDD
MTH1
β-actin
J
Inhibitor control
miR-4478 inhibitor
Mimics control
miR-4478 mimics
MTH1
β-actin
H2O2

Figure 3. Identification of MTH1 as a target gene for miR-4478. (A) Downregulated Gene Ontology (GO) terms with the most significant p values for biological processes, molecular function, and cellular component. (B) Weighted correlation network analysis (WGCNA) of the Gene Expression Omnibus (GEO) database (GSE70362). The topological overlaps of mRNA and their relations to modules were shown in the dendrogram. (C) Heatmap exhibiting the relationship between different gene modules and different degrees of disk degeneration (Pearson correlation). Purple modules were the most relevant to V grade degeneration. (D) Plot showing 21 genes in purple modules and their coexpression relationships. (E) Venn diagram showed predicted targets of miR-4478 by different algorithms. (F) The wild-type or mutant-type MTH1 3′ untranslated region reporter plasmid was cotransfected with miR-4478 mimics or mimics control into nucleus pulposus cells. Forty-eight hours after transfection, luciferase activity was measured (n = 3 replicates per group). $^{**}P < 0.01$. (G and H) Immunohistochemical staining of MTH1 and qualification analysis in nucleus pulposus tissues (IVDD = 12; control = 12). $^{****}P < 0.0001$. The $MTH1^{+}$ cells are pointed out by red arrows. (I) The expression levels of MTH1 in nucleus pulposus tissues were detected by western blot. (J) The expression levels of MTH1 in H_2O_2-induced intervertebral disk degeneration cell model which was pretransfected with miR-4478 mimics or inhibitor or their negative controls were detected by western blot. IVDD indicates intervertebral disk degeneration; MTH1, MutT homolog 1.

fissures, AF structure, AF clefts/fissures, and AF/NP boundary into evaluation. Each component was scored separately where a score of 0 represented a nondegenerated "normal" state, and the highest number indicating the highest level of changes observed. Individual scores were summed to give a final score, with a possible maximum of 14.

Statistical Analysis

Statistical analyses were performed using SPSS 23.0 software (IBM). One-way analysis of variance and Student *t* test were used to analyze the differences between groups. Typically, the results are presented as the mean ± SD, and *P* value <0.05 was considered statistically significant.

RESULTS

miR-4478 Was Upregulated in NP Tissues From IVDD Patients

To decipher the roles of miRNAs in IVDD, we first analyzed differentially expressed miRNAs with microarray datasets (GSE63492 and GSE116726) that were obtained from the Gene Expression Omnibus (GEO) database (Figure 1A, B). A mean fold change > 5 or <0.2 and *P* values <0.01 were taken as criteria, and then, dysregulated miRNAs obtained from the two microarray profiles were intersected to obtain the top 10 differentially expressed miRNAs (Figure 1C, D). Six upregulated miRNAs were tested by quantitative real-time polymerase chain reaction (qRT-PCR) using an independent cohort of 12 IVDD patients and 12 controls. miR-4478 was found to be significantly upregulated in NP tissues from IVDD patients compared with those from control patients (Figure 1F). Therefore, we selected miR-4478 for further investigation. And the finding was further confirmed by FISH (Figure 1G). These data suggest that miR-4478 may play an important role in the progression of IVDD.

Silencing of miR-4478 Inhibits H_2O_2-induced NPCs Apoptosis

To investigate the role of miR-4478 in the pathogenesis of IVDD, we conducted gain-of-function and loss-of-function studies. miR-4478 mimics and inhibitor were successfully constructed and transfected into primary human NPCs. We verified the transfection efficiency by qRT-PCR (Figure 2A). The CCK8 results demonstrated that upregulation of miR-4478 significantly decreased cell proliferation compared with the control group at 24, 48, and 72 hours; conversely, miR-4478 inhibitor transfection significantly increased cell proliferation (Figure 2B). Previous studies confirmed that the H_2O_2-induced IVDD cell model was reliable and that oxidative stress could induce IVDD both in vivo and in vitro[26,27] (Supplementary Figure 1, Supplemental Digital Content 1, http://links.lww.com/BRS/B924). miR-4478 mimics transfection markedly promoted the amounts of apoptosis in an H_2O_2-induced IVDD cell model (Figure 2C, D).

We further explored the effect of miR-4478 on apoptosis and oxidative stress-related markers. The expression of Bax and cleaved caspase 3 was increased in miR-4478 mimics transfected NPCs. In contrast, downregulation of miR-4478 highly increased the bcl-2 expression level (Figure 2E). In summary, these findings show that inhibition of miR-4478 could increase cell proliferation and suppress cell apoptosis.

Identification of MTH1 as a Target Gene for miR-4478

To identify the potential targets of miR-4478, Gene Ontology (GO) analysis and weighted gene coexpression network analysis (WGCNA) analysis were performed on the GEO database (GSE70362). Downregulated gene GO terms with the most significant *P* values for biological processes, cellular component, and molecular function were related to proteasomal protein catabolic process, an intrinsic component of organelle membrane, and ribonucleoprotein complex binding (Figure 3A). As for WGCNA results, 14 gene modules were discovered (Figure 3B). The relationships between gene modules and degrees of disk degeneration were discovered with Pearson correlation. Correlation coefficients (*r*) were illustrated as a heatmap (Figure 3C). Purple modules were positively correlated with V grade degeneration ($r = 0.41$). In addition, they were also negatively correlated with I grade degeneration ($r = -0.21$). The results demonstrated that genes in the purple modules could be viewed as IVDD suppressors. Patients with higher expression of genes in purple modules had lower degenerated NP tissues.

A $r > 0.5$ and makes up 0.75 of the modules were taken as criteria, and a total of 21 genes were found in purple modules (Figure 3D). Correlation analysis was performed with genes in the purple module. MTH1 was the most

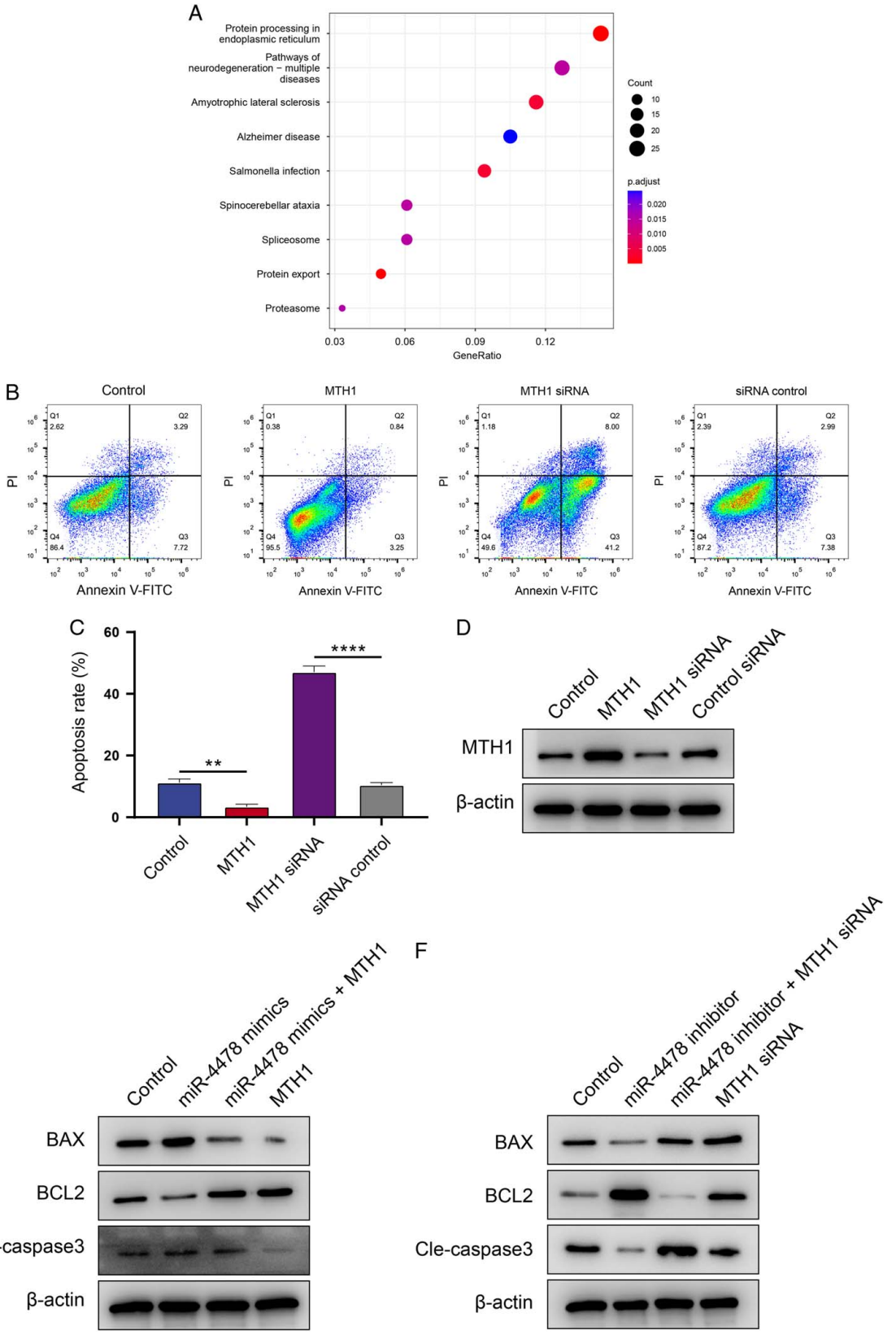
A
Protein processing in endoplasmic reticulum
Pathways of neurodegeneration – multiple diseases
Amyotrophic lateral sclerosis
Alzheimer disease
Salmonella infection
Spinocerebellar ataxia
Spliceosome
Protein export
Proteasome
0.03
0.06
0.09
0.12
GeneRatio
Count
10
15
20
25
p.adjust
0.020
0.015
0.010
0.005
B
Control
MTH1
MTH1 siRNA
siRNA control
PI
Annexin V-FITC
Q1 2.62
Q2 3.29
Q4 86.4
Q3 7.72
Q1 0.38
Q2 0.84
Q4 95.5
Q3 3.25
Q1 1.18
Q2 8.00
Q4 49.6
Q3 41.2
Q1 2.39
Q2 2.99
Q4 87.2
Q3 7.38
C
Apoptosis rate (%)
60
40
20
0
**
****
Control
MTH1
MTH1 siRNA
siRNA control
D
Control
MTH1
MTH1 siRNA
Control siRNA
MTH1
β-actin
E
Control
miR-4478 mimics
miR-4478 mimics + MTH1
MTH1
BAX
BCL2
Cle-caspase3
β-actin
F
Control
miR-4478 inhibitor
miR-4478 inhibitor + MTH1 siRNA
MTH1 siRNA
BAX
BCL2
Cle-caspase3
β-actin

Figure 4. miR-4478 regulates H_2O_2-induced nucleus pulposus cells (NPCs) apoptosis by modulating MutT homolog 1 (MTH1). (A) Kyoto Encyclopedia of Genes and Genomes (KEGG) analysis demonstrating "Protein processing in endoplasmic reticulum" enriched in intervertebral disk degeneration. (B and C) Analysis of NPCs apoptosis was assayed by flow cytometry (n = 3 replicates per group). Human recombinant MTH1 suppressed H_2O_2-induced apoptosis in NPCs. Meanwhile, silencing of MTH1 expression promoted H_2O_2-induced apoptosis in NPCs. $^{**}P < 0.01$, $^{****}P < 0.0001$. (D) NPCs were transfected with control siRNA, or MTH1 siRNA for 72 hours or treated with human recombinant MTH1 for 48 hours, and then the expression levels of BAX, BCL2, and cleaved caspase 3 were measured by western blot. (E) Upregulation of BAX and cleaved caspase 3 expression levels by miR-4478 mimics was compressed by extrinsic MTH1. What's more, downregulation of BCL2 expression level by miR-4478 mimics was increased by MTH1 overexpression. (F) Downregulation of BAX and cleaved caspase 3 expression levels by miR-4478 inhibitor in the H_2O_2-induced intervertebral disk degeneration cell model was abolished by silencing of MTH1 expression. In comparison, upregulation of BCL2 expression levels by miR-4478 inhibitor was reduced by MTH1 downregulation.

relevant gene for the degree of disk degeneration using the Kaplan-Meier method according to log-rank *P* values.

Subsequently, a Venn analysis was performed to show all the predicted genes with different algorithms (Figure 3E). To verify our prediction, the putative binding sites were evaluated by luciferase reporter assay analysis (Figure 3F, Supplementary Figure 2, Supplemental Digital Content 1, http://links.lww.com/BRS/B924). Consistent with these findings, the expression level of MTH1 in IVDD NP tissues was lower than that in the control group (Figure 3G, H). The result was further confirmed by western blot (Figure 3I, J). These results demonstrate that MTH1 is a target gene of miR-4478.

miR-4478 Regulates H_2O_2-induced NPCs Apoptosis by Modulating MTH1

A Kyoto Encyclopedia of Genes and Genomes (KEGG) analysis was performed on the above-mentioned predicted targets of miR-4478, and "Protein processing in endoplasmic reticulum" was enriched in IVDD (Figure 4A). To further analyze the underlying mechanism by how MTH1 regulates H_2O_2-induced NPCs apoptosis, we first established MTH1 small interfering RNA (siRNA) to suppress the expression of MTH1, and the transfection efficiency was detected by western blot (Figure 4B, D). Cultured NPCs were transfected with MTH1 siRNA or its negative control or treated with human recombinant MTH1 to simulate MTH1 overexpression. Flow cytometry results showed that transfection with MTH1 siRNA promoted apoptosis in an H_2O_2-induced IVDD cell model. Conversely, the amount of apoptosis was decreased in the human recombinant MTH1 treatment group (Figure 4B, C).

Subsequently, to further demonstrate the underlying mechanism of MTH1-regulated apoptosis, cultured NPCs were transfected with miR-4478 mimics or its negative control or treated with human recombinant MTH1. The expression levels of Bax and cleaved caspase 3 were significantly upregulated in H_2O_2-treated NPCs transfected with miR-4478 mimics. In contrast, the expression levels of Bcl-2 were lower than those in the H_2O_2 treatment group (aka "control group") (Figure 4E). These results imply that silencing MTH1 may aggravate H_2O_2-induced oxidative stress in NPCs. Furthermore, MTH1 siRNA had effects on Bax, Bcl-2, and cleaved caspase 3 expressions similar to the effects induced by miR-4478 (Figure 4F).

These data indicate that miR-4478 regulates H_2O_2-induced NPCs apoptosis by modulating MTH1.

Downregulation of miR-4478 Alleviated IVDD in a Mouse Model

To clarify whether miR-4478 could become an effective target for biological therapy of IVDD, we administrated a miR-4478 inhibitor or its negative control to an AF puncture-induced IVDD mouse model. Local injection of miR-4478 inhibitor solution significantly alleviated the degeneration of IVDs, as shown by imaging manifestations and histological observations (Figure 5A–D). In addition, immunohistochemical results demonstrated that the expression level of MTH1 was reversed in the miR-4478 inhibitor group compared with the IVDD mouse model or inhibitor control group (Figure 5E, F).

These results indicate that downregulation of miR-4478 had a protective role in the progression of IVDD, implying miR-4478 as a potential target for biological therapy of IVDD.

DISCUSSION

miRNAs are a class of small noncoding RNAs of ~22 nucleotides in length that play a crucial role in the post-transcriptional regulation of protein expression. Many studies have demonstrated that abnormal miRNA expression is related to cell apoptosis, proliferation, differentiation, transformation, and migration.[28–31] There is accumulating evidence indicating that miRNAs are associated with the progression of IVDD, revealing that the pathogenesis of IVDD may help to relieve the clinical and socioeconomic burden imposed on modern society.[32]

In this study, we first identified that miR-4478 was downregulated in NP tissues of IVDD patients. Then, bioinformatic analyses were performed to determine that MTH1 is a target gene of miR-4478, which was later confirmed by dual-luciferase analysis. Therefore, we hypothesized that miR-4478 may function by modulating MTH1 in IVDD progression. This study showed that the overexpression of miR-4478 remarkably increased H_2O_2-induced NPCs apoptosis, indicating a harmful effect of miR-4478 on NPCs survival under oxidative stress. In addition, subsequent animal experiments demonstrated that the downregulation of miR-4478 alleviated surgery-induced IVDD in a mouse model in vivo. These data suggest that the upregulation of miR-4478 may contribute to IVDD progression, and suppressing miR-4478 expression in vivo might be an effective strategy for treating IVDD.

We noticed that miRNA studies on IVDD have been springing up in recent years, and several miRNAs have been identified to be involved in the development of IVDD.[33–38] However, these findings have not come to a consistent

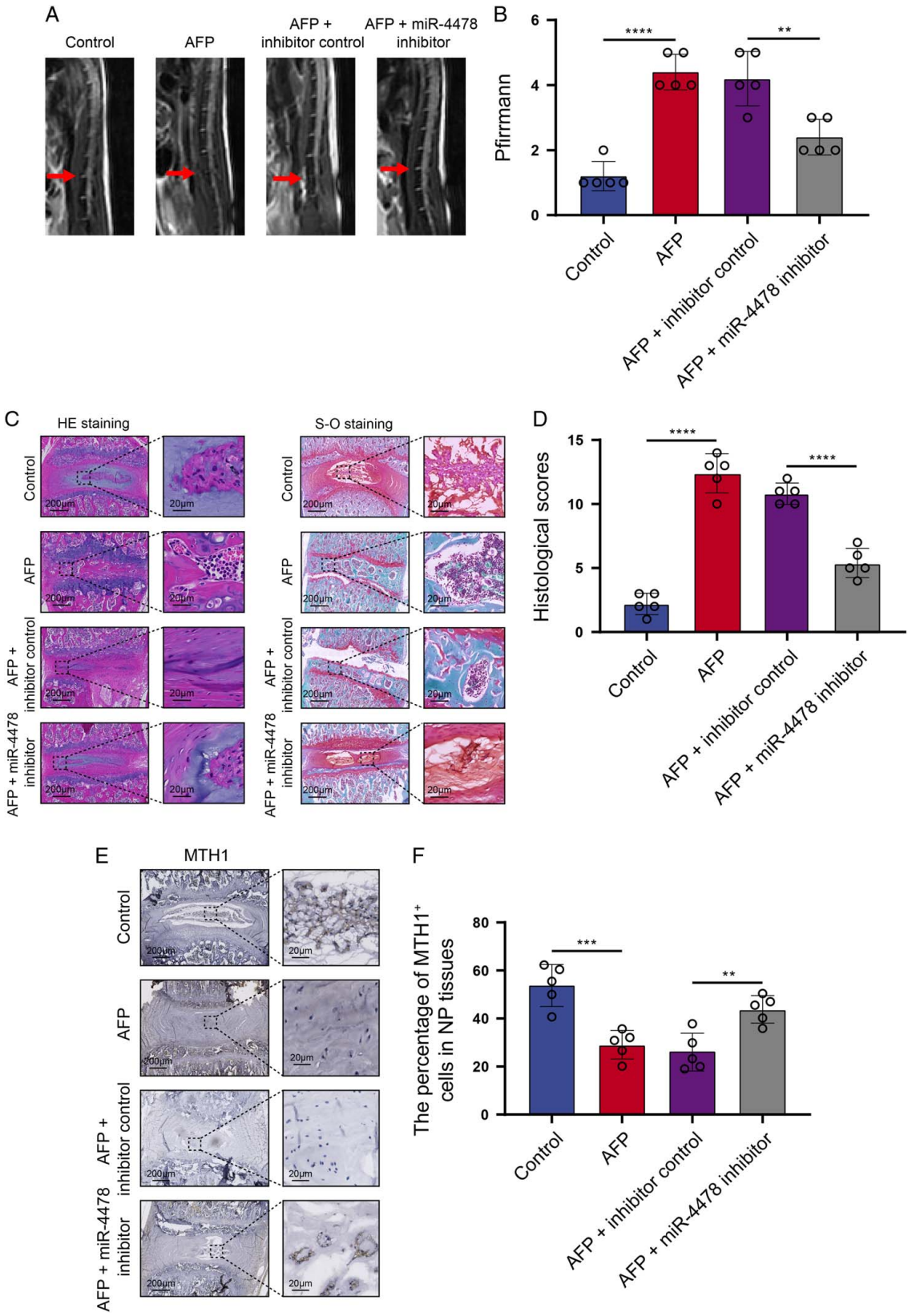

Figure 5. Downregulation of miR-4478 alleviated intervertebral disk degeneration in a mouse model. (A and B) The intervertebral disk degeneration evaluated by magnetic resonance images after eight weeks of surgery and quantitative analysis based on Pfirrmann grading was performed. $^{**}P < 0.01$, $^{****}P < 0.0001$. (C and D) The representative images of HE staining and Safranin O. Histological scores of different groups were analyzed. $^{****}P < 0.0001$. (E and F) Immunohistochemical staining for MTH1 and qualification analysis in intervertebral disk degeneration model treated by miR-4478 inhibitor at eight weeks (magnification: ×400). Data shown as mean ± SD (n = 5). AFP indicates annulus fibrosus puncture; HE, hematoxylin and eosin; MTH1, MutT homolog 1.

conclusion regarding the explicit pathogenesis of IVDD.[39–43] Although miR-4478 has been reported to be able to promote cell proliferation and migration in many diseases, this is the first study to identify miR-4478 as a key regulator in the pathogenesis of IVDD. In our study, miR-4478 was identified as a key factor in IVDD by microarray dataset analysis, as confirmed by qRT-PCR and FISH analysis. In addition, we showed that high miR-4478 expression strongly correlates with advanced degeneration of IVDs. miR-4478 promoted the amount of NPCs apoptosis induced by oxidative stress. These results suggest the possibility of miR-4478 as a therapeutic target for IVDD treatment.

A growing number of studies have shown that oxidative stress plays an important role in the pathogenesis of IVDD.[44–49] ROS can act as signaling molecules in several cell types to regulate signaling pathways; for example, H_2O_2 is involved in the regulation of the NF-κB and MAPK pathways.[6] There are a variety of endogenous antioxidants and protective factors that protect cells from oxidative stress damage. MTH1 overexpression has been studied in several cancers, including lung cancer, gastric cancer, and esophageal squamous cell carcinomas.[50–55] These results indicate that MTH1 may influence the proliferation, apoptosis and differentiation of tumor cells.[56–58] However, the role of MTH1 in IVDD progression is still unknown. In the present study, we identified MTH1 as a target gene of miR-4478 in NPCs. Human recombinant MTH1 inhibited the proapoptotic and proinflammatory functions of miR-4478 in an H_2O_2-induced IVDD cell model. Our data suggest that MTH1 regulates cell apoptosis, which is a pathological hallmark of IVDD. The GO terms associated with MTH1 in NPCs include proteasomal protein catabolic process, an intrinsic component of organelle membrane, and ribonucleoprotein complex binding. However, further investigations are necessary to determine the relationship between these biological pathways and MTH1 in IVDD.

However, this study has its limitations in that human IVDs samples incorporated in this study were in a similar age cohort, and it may result in bias leaded by the difference between the average age of the control group and the IVDD group. Regrettably, we do not have enough human clinical specimens to perform the above-mentioned experiments, which will be beneficial for consolidating the association of miR-4478 expression with IVDD. Although the therapeutic effect of the miR-4478 inhibitor in a surgery-induced IVDD mouse model was effective, the optimal dose remains to be determined, and the side effects are still unknown. There are still several problems to be solved, and many hurdles to overcome before it is administered to humans. Meanwhile, the downstream signaling pathway by which MTH1 regulates oxidative stress-induced NPCs apoptosis remains unclear. Further studies are required to elucidate the role of the miR-4478/MTH1 axis in modulating the pathogenesis of IVDD.

CONCLUSIONS

Our studies demonstrate that the expression level of miR-4478 in NP tissues is positively correlated with the disk degeneration grade and identify MTH1 as a direct gene target of miR-4478. Moreover, we found that MTH1 protected NPCs against oxidative stress induced by H_2O_2 and that miR-4478 promoted H_2O_2-induced NPCs apoptosis by regulating the MTH1 expression level. Overall, our results provide the possibility of applying miR-4478-based therapy to treat IVDD patients in the clinic.

➢ Key Points

- ❑ miR-4478 was upregulated in NP tissues from IVDD patients.
- ❑ Silencing of miR-4478 inhibited H_2O_2-induced NPCs apoptosis.
- ❑ MTH1 was identified as a target gene for miR-4478.
- ❑ miR-4478 regulated H_2O_2-induced NPCs apoptosis by modulating MTH1.
- ❑ Downregulation of miR-4478 alleviated IVDD in a mouse model.

Reference

1. Knezevic NN, Candido KD, Vlaeyen JWS, Van Zundert J, Cohen SP. Low back pain. *Lancet*. 2021;398:78–92.
2. Deyo RA, Mirza SK. Clinical practice. Herniated lumbar intervertebral disk. *N Engl J Med*. 2016;374:1763–72.
3. Hartvigsen J, Hancock MJ, Kongsted A, et al. What low back pain is and why we need to pay attention. *Lancet*. 2018;391:2356–67.
4. Ramaswami R, Ghogawala Z, Weinstein JN. Management of sciatica. *N Engl J Med*. 2017;376:1175–7.
5. Binch ALA, Fitzgerald JC, Growney EA, Barry F. Cell-based strategies for IVD repair: clinical progress and translational obstacles. *Nat Rev Rheumatol*. 2021;17:158–75.
6. Chen F, Jiang G, Liu H, et al. Melatonin alleviates intervertebral disc degeneration by disrupting the IL-1β/NF-κB-NLRP3 inflammasome positive feedback loop. *Bone Res*. 2020;8:10.
7. Yang S, Zhang F, Ma J, Ding W. Intervertebral disc ageing and degeneration: the antiapoptotic effect of oestrogen. *Ageing Res Rev*. 2020;57:100978.
8. Bartel DP. MicroRNAs: target recognition and regulatory functions. *Cell*. 2009;136:215–33.
9. Cheng X, Zhang L, Zhang K, et al. Circular RNA VMA21 protects against intervertebral disc degeneration through targeting miR-200c and X linked inhibitor-of-apoptosis protein. *Ann Rheum Dis*. 2018;77:770–9.
10. Ji M-L, Jiang H, Zhang X-J, et al. Preclinical development of a microRNA-based therapy for intervertebral disc degeneration. *Nat Commun*. 2018;9:5051.
11. Zhang W-L, Chen Y-F, Meng H-Z, et al. Role of miR-155 in the regulation of MMP-16 expression in intervertebral disc degeneration. *J Orthop Res*. 2017;35:1323–34.
12. Gad H, Koolmeister T, Jemth A-S, et al. MTH1 inhibition eradicates cancer by preventing sanitation of the dNTP pool. *Nature*. 2014;508:215–21.
13. Kohno Y, Yamamoto H, Hirahashi M, et al. Reduced MUTYH, MTH1, and OGG1 expression and TP53 mutation in diffuse-type adenocarcinoma of gastric cardia. *Hum Pathol*. 2016;52:145–52.
14. Liou G-Y, Storz P. Reactive oxygen species in cancer. *Free Radic Res*. 2010;44:479–96.
15. Lushchak VI. Free radicals, reactive oxygen species, oxidative stress and its classification. *Chem Biol Interact*. 2014;224:164–75.
16. Obtulowicz T, Swoboda M, Speina E, et al. Oxidative stress and 8-oxoguanine repair are enhanced in colon adenoma and carcinoma patients. *Mutagenesis*. 2010;25:463–71.

17. Nakabeppu Y, Ohta E, Abolhassani N. MTH1 as a nucleotide pool sanitizing enzyme: friend or foe? *Free Radic Biol Med*. 2017;107:151–8.
18. Agarwal V, Bell GW, Nam JW, Bartel DP. Predicting effective microRNA target sites in mammalian mRNAs. *eLife*. 2015;4: e05005.
19. Sticht C, De La Torre C, Parveen A, Gretz N. miRWalk: an online resource for prediction of microRNA binding sites. *PLoS ONE*. 2018;13:e0206239.
20. Liu W, Wang XJ. Prediction of functional microRNA targets by integrative modeling of microRNA binding and target expression data. *Genome Biol*. 2019;20:18.
21. Yu X, Liu Q, Wang Y, Bao Y, Jiang Y, Li M, et al. Depleted long noncoding RNA GAS5 relieves intervertebral disc degeneration via microRNA-17-3p/Ang-2. *Oxid Med Cell Longev*. 2022;2022:1792412.
22. Xiao Z-F, Su G-Y, Hou Y, Chen S-D, Zhao B-d, He J-B, et al. Mechanics and biology interact in intervertebral disc degeneration: a novel composite mouse model. *Calcif Tissue Int*. 2020;106:401–14.
23. Martin JT, Gorth DJ, Beattie EE, Harfe BD, Smith LJ, Elliott DM. Needle puncture injury causes acute and long-term mechanical deficiency in a mouse model of intervertebral disc degeneration. *J Orthop Res*. 2013;31:1276–82.
24. Zhang H, Yao S, Zhang Z, Zhou C, Fu F, Bian Y, et al. Network pharmacology and experimental validation to reveal the pharmacological mechanisms of liuwei dihuang decoction against intervertebral disc degeneration. *Drug Des Devel Ther*. 2021;15:4911–24.
25. Tam V, Chan WCW, Leung VYL, Cheah KSE, Cheung KMC, Sakai D, et al. Histological and reference system for the analysis of mouse intervertebral disc. *J Orthop Res*. 2018;36:233–43.
26. Cheng X, Lin J, Chen Z, Mao Y, Wu X, Xu C, et al. CB2-mediated attenuation of nucleus pulposus degeneration via the amelioration of inflammation and oxidative stress in vivo and in vitro. *Mol Med*. 2021;27:92.
27. Lin J, Du J, Wu X, Xu C, Liu J, Jiang L, et al. SIRT3 mitigates intervertebral disc degeneration by delaying oxidative stress-induced senescence of nucleus pulposus cells. *J Cell Physiol*. 2021;236:6441–56.
28. Huang Z, Shi T, Zhou Q, et al. miR-141 Regulates colonic leukocytic trafficking by targeting CXCL12β during murine colitis and human Crohn's disease. *Gut*. 2014;63:1247–57.
29. Mateescu B, Batista L, Cardon M, et al. miR-141 and miR-200a act on ovarian tumorigenesis by controlling oxidative stress response. *Nat Med*. 2011;17:1627–35.
30. Wang L, Liu Y, Li H, et al. sensitizes ovarian cancer cells to irradiation by inhibiting and attenuating autophagy. *Mol Ther Nucleic Acids*. 2021;23:1110–9.
31. Zhou X, Xie D, Huang J, et al. Therapeutic effects of (5R)-5-hydroxytriptolide on fibroblast-like synoviocytes in rheumatoid arthritis lncRNA WAKMAR2/miR-4478/E2F1/p53 Axis. *Front Immunol*. 2021;12:605616.
32. Xie L, Huang W, Fang Z, et al. CircERCC2 ameliorated intervertebral disc degeneration by regulating mitophagy and apoptosis through miR-182-5p/SIRT1 axis. *Cell Death Dis*. 2019;10:751.
33. Sun J-C, Zheng B, Sun R-X, et al. MiR-499a-5p suppresses apoptosis of human nucleus pulposus cells and degradation of their extracellular matrix by targeting SOX4. *Biomed Pharmacother*. 2019;113:108652.
34. Zhang J, Zhang J, Zhang Y, et al. Mesenchymal stem cells-derived exosomes ameliorate intervertebral disc degeneration through inhibiting pyroptosis. *J Cell Mol Med*. 2020;24:11742–54.
35. Zhang S, Song S, Zhuang Y, et al. Role of microRNA-15a-5p/Sox9/NF-κB axis in inflammatory factors and apoptosis of murine nucleus pulposus cells in intervertebral disc degeneration. *Life Sci*. 2021;277:119408.
36. Sun Y, Wang X, Fu G, Geng X. MicroRNA-199a-5p accelerates nucleus pulposus cell apoptosis and IVDD by inhibiting SIRT1-mediated deacetylation of p21. *Mol Ther Nucleic Acids*. 2021;24: 634–45.
37. Bao X, Wang Z, Jia Q, et al. HIF-1-mediated miR-623 regulates apoptosis and inflammatory responses of nucleus pulposus induced by oxidative stress via targeting TXNIP. *Oxid Med Cell Longev*. 2021;2021:6389568.
38. Sun Y, Zhang W, Li X. Induced pluripotent stem cell-derived mesenchymal stem cells deliver exogenous miR-105-5p via small extracellular vesicles to rejuvenate senescent nucleus pulposus cells and attenuate intervertebral disc degeneration. *Stem Cell Res Ther*. 2021;12:286.
39. Wang H, Tian Y, Wang J, et al. Inflammatory cytokines induce NOTCH signaling in nucleus pulposus cells: implications in intervertebral disc degeneration. *J Biol Chem*. 2013;288:16761–74.
40. Ji M-L, Zhang X-J, Shi P-L, et al. Downregulation of microRNA-193a-3p is involved in invertebral disc degeneration by targeting MMP14. *J Mol Med (Berl)*. 2016;94:457–68.
41. Lu J, Ji M-L, Zhang X-J, et al. MicroRNA-218-5p as a potential target for the treatment of human osteoarthritis. *Mol Ther*. 2017;25:2676–88.
42. Risbud MV, Shapiro IM. Role of cytokines in intervertebral disc degeneration: pain and disc content. *Nat Rev Rheumatol*. 2014;10:44–56.
43. Nasto LA, Seo H-Y, Robinson AR, et al. ISSLS prize winner: inhibition of NF-κB activity ameliorates age-associated disc degeneration in a mouse model of accelerated aging. *Spine (Phila Pa 1976)*. 2012;37:1819–25.
44. Che H, Li J, Li Y, et al. p16 deficiency attenuates intervertebral disc degeneration by adjusting oxidative stress and nucleus pulposus cell cycle. *eLife*. 2020;9:e52570.
45. He R, Cui M, Lin H, et al. Melatonin resists oxidative stress-induced apoptosis in nucleus pulposus cells. *Life Sci*. 2018;199: 122–30.
46. Sun K, Jing X, Guo J, Yao X, Guo F. Mitophagy in degenerative joint diseases. *Autophagy*. 2021;17:2082–92.
47. Xie L, Chen Z, Liu M, et al. MSC-derived exosomes protect vertebral endplate chondrocytes against apoptosis and calcification via the miR-31-5p/ATF6 Axis. *Mol Ther Nucleic Acids*. 2020;22:601–14.
48. Yang R-Z, Xu W-N, Zheng H-L, et al. Involvement of oxidative stress-induced annulus fibrosus cell and nucleus pulposus cell ferroptosis in intervertebral disc degeneration pathogenesis. *J Cell Physiol*. 2021;236:2725–39.
49. Zhang X, Huang Z, Xie Z, et al. Homocysteine induces oxidative stress and ferroptosis of nucleus pulposus via enhancing methylation of GPX4. *Free Radic Biol Med*. 2020;160:552–65.
50. Yin Y, Chen F. Targeting human MutT homolog 1 (MTH1) for cancer eradication: current progress and perspectives. *Acta Pharm Sin B*. 2020;10:2259–71.
51. Ou Q, Ma N, Yu Z, et al. Nudix hydrolase 1 is a prognostic biomarker in hepatocellular carcinoma. *Aging*. 2020;12:7363–79.
52. Samaranayake GJ, Huynh M, Rai P. MTH1 as a chemotherapeutic target: the elephant in the room. *Cancers (Basel)*. 2017;9:47.
53. Zhou W, Ma L, Yang J, et al. Potent and specific MTH1 inhibitors targeting gastric cancer. *Cell Death Dis*. 2019;10:434.
54. Moukengue B, Brown HK, Charrier C, et al. TH1579, MTH1 inhibitor, delays tumour growth and inhibits metastases development in osteosarcoma model. *EBioMedicine*. 2020;53:102704.
55. Magkouta SF, Pappas AG, Vaitsi PC, et al. MTH1 favors mesothelioma progression and mediates paracrine rescue of bystander endothelium from oxidative damage. *JCI Insight*. 2020;5:e134885.
56. Farand J, Kropf JE, Blomgren P, et al. Discovery of potent and selective MTH1 inhibitors for oncology: enabling rapid target (in) validation. *ACS Med Chem Lett*. 2020;11:358–64.
57. Warpman Berglund U, Sanjiv K, Gad H, et al. Validation and development of MTH1 inhibitors for treatment of cancer. *Ann Oncol*. 2016;27:2275–83.
58. Samaranayake GJ, Troccoli CI, Zhang L, et al. The existence of MTH1-independent 8-oxodGTPase activity in cancer cells as a compensatory mechanism against on-target effects of MTH1 inhibitors. *Mol Cancer Ther*. 2020;19:432–46.